JOC The Journal of Organic Chemistry

Article

pubs.acs.org/joc

Mechanistic Insights on Organocatalytic Enantioselective Decarboxylative Protonation by Epicinchona-Thiourea Hybrid Derivatives

Arkajyoti Sengupta and Raghavan B. Sunoj*

Department of Chemistry, Indian Institute of Technology Bombay, Powai, Mumbai 400076, India

Supporting Information

ABSTRACT: Mechanism and the origin of enantioselectivity in the decarboxylative protonation of α-amino malonate hemiester promoted by epicinchona−thiourea hybrid organocatalyst is established by using the DFT(M06-2X/6-311+G**//ONIOM2) computational methods. The origin of stereoselectivity rendered by this hybrid bifunctional catalyst in asymmetric protonation is investigated for the first time using suitable transition-state models. A detailed conformational analysis of *N*-[3,5-bis(trifluoromethyl)]phenylthiourea-based epicinchonidine reveals the potential for a bifunctional mode of activation of the substrate α-amino malonate hemiester through hydrogen bonding. Six different conformer families differing in characteristic dihedral angles are identified within a range of 16 kcal/mol with respect to the lowest energy conformer. Different likely mechanistic pathways obtained through detailed analysis of the transition states and intermediates are compared. It is identified that in the preferred pathway, the decarboxylation is followed by a direct proton transfer from the chiral quinuclidinium moiety to the enolate carbon as opposed to a conventional protonation at the enolate oxygen followed by a keto−enol tautomerization. The factors responsible for high levels of observed stereoselectivity are traced to interesting hydrogen-bonding interactions offered by the thiourea−cinchona bifunctional framework. The predicted stereoselectivities using computed Gibbs free energies of diastereomeric transition states are in fair agreement with the experimental stereoselectivities.

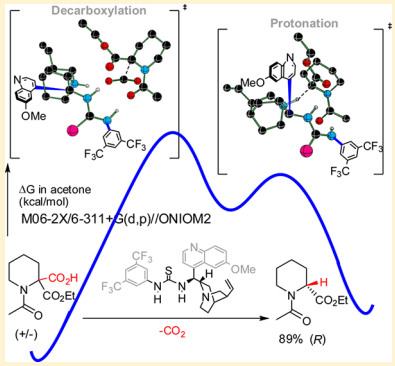

INTRODUCTION

Among the richly diverse family of organocatalysts that are in use today, cinchona alkaloids and their derivatives are known to promote a range of synthetically important reactions, often with excellent stereoselectivities.[1] The naturally occurring cinchona variant contains multiple functional groups besides possessing five stereogenic centers. Such alkaloids exhibit potential for asymmetric catalysis owing to their chiral recognition capabilities, structural diversity, and conformational features.[2] Mechanistic studies have revealed two key attributes that generally work in tandem for this class of bifunctional organocatalysts. These include (a) the Lewis or Bronsted basicity of quinuclidine nitrogen[3] toward deprotonating a pro-nucleophile and (b) the hydrogen bond donor group (OH) capable of providing simultaneous activation of the electrophilic partner.[4]

The developments in chemical catalysis have always derived inspiration from enzyme catalysis.[5] The domain of organocatalysis remained no exception to this trend. One such example is in the use of thiourea and its variants as organocatalysts,[6] wherein a network of hydrogen-bonding interactions with a range of Lewis bases is exploited.[7] The seminal contributions on chiral (thio)urea derivatives by Jacobsen,[8] Schreiner,[9] Takemoto,[10] Chen,[11] and Soos[12] provided timely impetus for its increasingly popularity. A select set of examples is succinctly summarized in Chart 1 to bring out the versatility of applications of thiourea derivatives in a diverse set of reactions. The covalent linkage between naturally available cinchona alkaloids and thiourea has given rise to improved hybrid catalysts. Such thiourea−cinchona hybrid catalysts offer more tunability in H-bond donor groups in addition to providing bifunctional activation of substrates.[13]

Computational methods have generally been effective toward understanding the mechanism of thiourea-based organocatalysts.[14] Despite the above-mentioned advances and the broad interest in bifunctional thiourea cinchona alkaloids, several mechanistic issues continue to remain unsettled. Cinchona alkaloids are conformationally flexible and could therefore exist as a mixture of conformers. A key issue that impedes gaining deeper molecular insights on the mechanism is the lack of structural information, including conformational states and dynamics.

In one recent application, a hybrid thiourea−cinchona template has been demonstrated as being capable of offering a high degree of enantioselectivity in an asymmetric decarboxylative protonation reaction.[15] A racemic mixture of α-amino malonate hemiester has been converted to enantiomerically enriched α-amino esters with the highest enantioselectivity to date with any chiral organic base (Scheme 1). The reaction is suggested to be a promising strategy for the synthesis of natural and non-natural α-amino acids. From a mechanistic standpoint,

Received: July 13, 2012
Published: November 15, 2012

Chart 1. Select Examples of Commonly Used Organocatalysts Derived from Thiourea

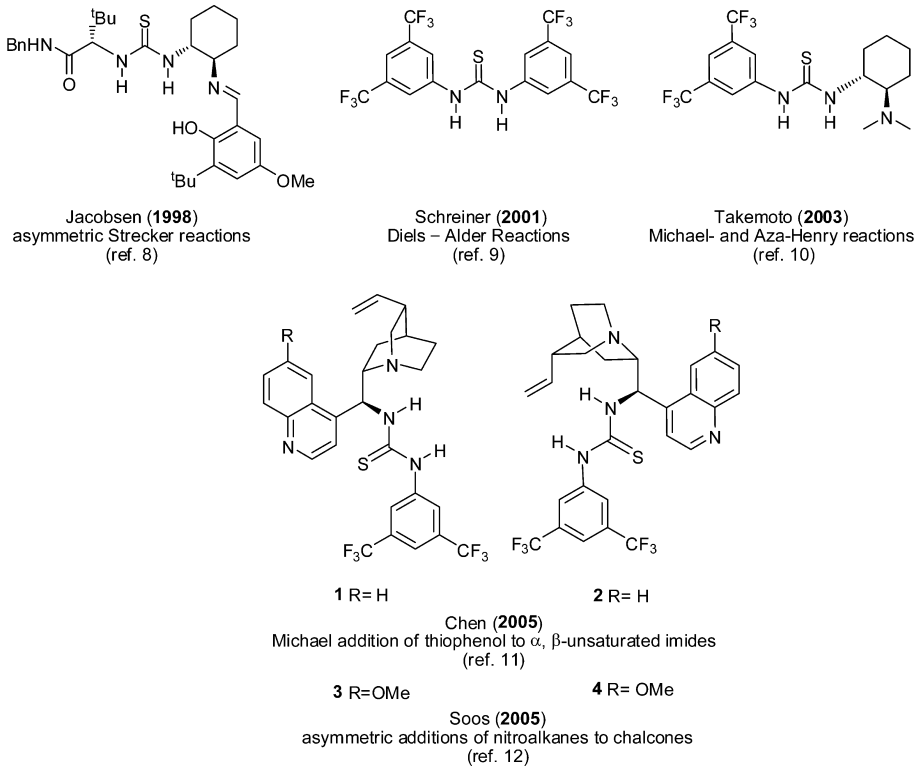

Scheme 1. Hybrid Thiourea−Cinchona Template Mediating Asymmetric Decarboxylative Protonation

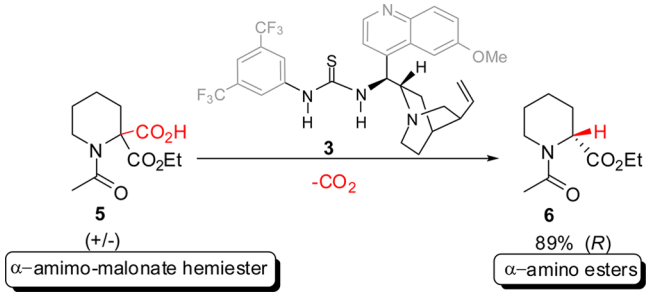

the significance of this reaction is higher as stereoselective protonation reactions are relatively rarerer.[16] The general reliance on steric factors as control elements in stereoselective reactions may not translate well to an asymmetric protonation reaction. As part of our continued interest in establishing the molecular origin of stereoselectivity in organic reactions,[17] we have undertaken a detailed mechanistic investigation on enantioselective decarboxylative protonation of malonate hemiesters. The key objectives include the identification of (a) lower energy conformers that can form binary adducts with the substrate, (b) mechanism of decarboxylation and asymmetric protonation in such binary adducts, and (c) factors that contribute to high levels of enantioselectivity in this reaction.

COMPUTATIONAL METHODS

The present system consisting of hybrid thiourea−cinchona alkaloid and the substrate is quite large and complex from a computational standpoint, both in terms of number of atoms and the likely conformational possibilities. Hence, application of full DFT computations to address numerous problems would naturally be more resource demanding. Since we aim to examine the reaction mechanism and stereoselectivity issues, a hybrid QM/QM method has been employed. There have been a number of successful applications of such hybrid calculations for larger molecular systems.[18] We have employed Morokuma's ONIOM2 partition scheme wherein the site of reaction as well as the immediate neighborhood is explicitly treated with a quantum mechanical model (higher layer) while the groups/arms, which are expected to have only an indirect influence on the reaction, are treated using a semiempirical model (lower layer). The partition scheme employed in the present study is shown using atoms of lighter and darker colored shades, respectively, for lower and higher layer in Figure 1. Recent studies have suggested that semiempirical methods perform quite well as a lower layer than the commonly used molecular mechanics (MM) methods.[19] This is due to the improved ability of semiempirical formalism to account for the polarization of electron density between the lower and higher layers as compared to when the lower layer is represented using the MM method.

We have therefore used a combination of density functional theory (mPW1PW91/6-311G**) and semiempirical MO methods (PM3) in the ONIOM2 scheme,[20] denoted as ONIOM2(mPW1PW91/6-311G**:PM3) for the conformational analysis of the alkaloid derivative using the Gaussian09 suite of quantum chemical programs.[21] In the ONIOM2(mPW1PW91/6-311G**:PM3) approach, the energy of the real system at the high level was estimated using an extrapolation scheme: $E_{(\mathrm{ONIOM})} = E_{(\mathrm{high,\ model})} + E_{(\mathrm{low,\ real})} - E_{(\mathrm{low,\ model})}$.[22] This approach has been successful in rationalizing the mechanism as well as stereoselectivity of organic reactions.[17b,23] The geometry optimizations of thiourea-cinchona template, various intermediates, and the interconnecting transition states were carried out using the ONIOM2 method described above. All the transition states were characterized as possessing one and only one imaginary frequency characteristic of a true first order saddle point. The identity of these transition states was further confirmed as representing the desired reaction coordinate by using intrinsic reaction coordinate (IRC) analysis.

In accordance with the recommendations of Morokuma et al. for a multilayer hybrid calculation, a substituent value test (*S*-value test) was performed[24] for the present set of substrates.[25] The *S*-value test was to examine the goodness of the partition scheme and the corresponding model chemistries. The computed values indicated that among various

dx.doi.org/10.1021/jo301483p | J. Org. Chem. 2012, 77, 10525−10536

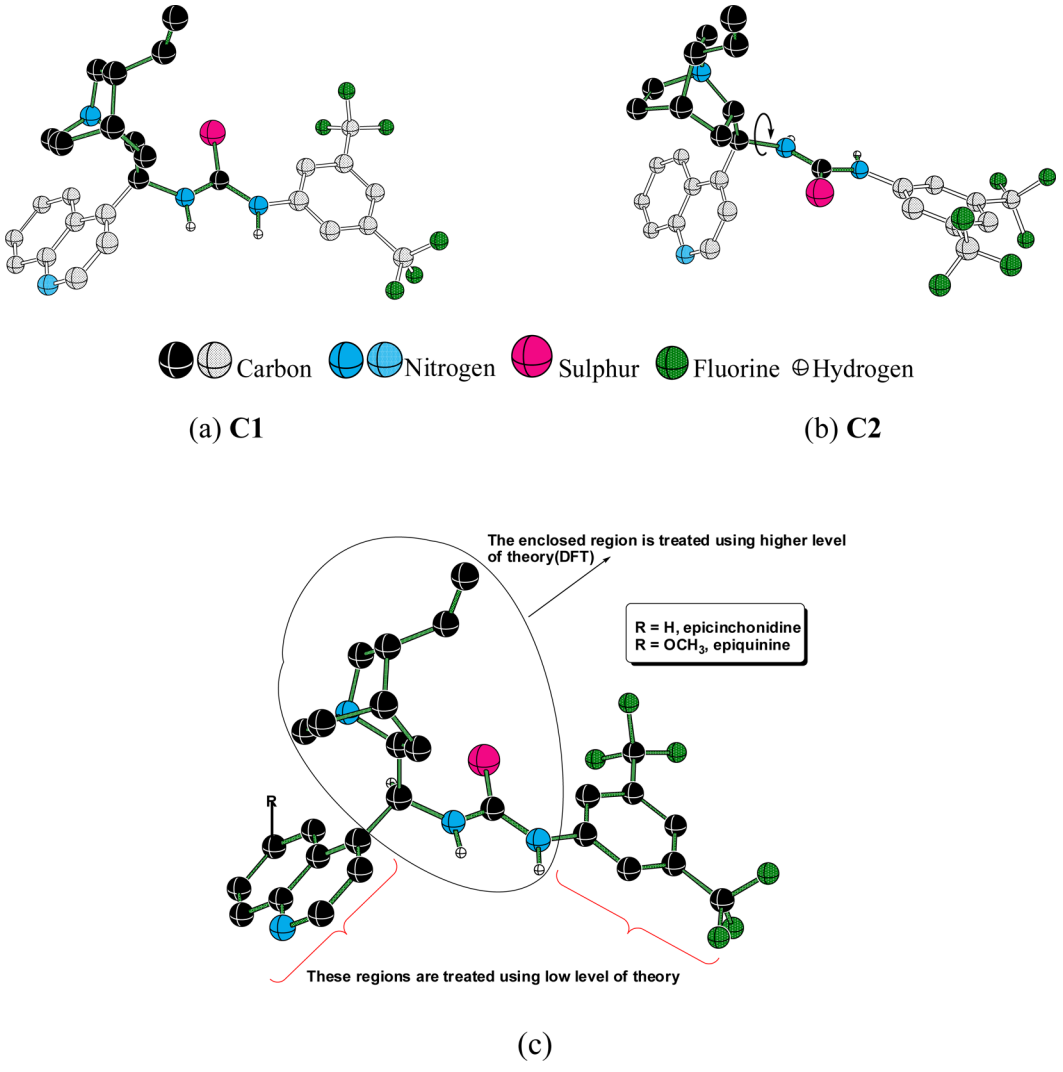

Figure 1. ONIOM2(mPW1PW91/6-311G**:PM3) optimized geometries of two key conformers **C1** and **C2** of epicinchonidine derivative **1** (a and b). Lighter gray and darker colored shadings, respectively, represent the lower (PM3) and higher (mPW1PW91) layers in the ONIOM2 partitioning. (c) The description of higher and lower layers employed in the ONIOM2 computations.

partition schemes employed, ONIOM2(mPW1PW91/6-311G**:PM3) was found to be the most suitable scheme for the present problem, and therefore, the results of conformational analyses are presented on the basis of the geometries obtained using this method. The mechanistic studies were performed with a basis set consisting of diffuse functions at the ONIOM2(mPW1PW91/6-31+G**:PM3) level of theory. The solvent effects arising due to acetone continuum (ε = 20.49) were then incorporated using the continuum solvation model with the SCRF-SMD framework as formulated by Truhlar and Cramer.[26] The zero-point vibrational energy (ZPVE) and thermal and entropic terms obtained using the gas-phase calculations at the ONIOM2(mPW1PW91/6-31+G**:PM3) level of theory are added to the single-point energies in the continuum dielectric (solvent = acetone, ε = 20.49) evaluated at the mPW1PW91/6-31+G** as well as the M06−2X/6-311+G** levels. The Gibbs free energies in the solvent phase obtained at the $SMD_{(acetone)}$/M06-2X/6-311+G-(d,p)//ONIOM2(mPW1PW91/6-31+G**:PM3) level of theory are employed for discussions of the mechanistic investigations. This quantity includes thermal and entropic terms estimated using standard statistical mechanics approximations (harmonic oscillator and rigid rotor) in the gas phase at the ONIOM2 level.

Two-Layer ONIOM Partitioning. The epicinchonidine thiourea derivative **1** (Chart 1) can give rise to many more conformers than its parent alkaloid due to the additional rotational degrees of freedom generated by substitution of −OH by a phenylthiourea moiety. Two of the key conformers **C1** and **C2** (vide infra), as shown in Figure 1, were first taken as a representative set toward calculating the relative energies when different partition schemes are employed. The energy differences were evaluated using the ONIOM partitioning schemes that differ in terms of the DFT and the semiempirical methods employed, respectively, for the higher and lower layers. The ΔS-value and the corresponding difference in the ONIOM extrapolation energy error (ΔD) for each such combination were obtained by using relative energies of these two conformers (see Table S1 in the Supporting Information). The quantity ΔD computed as the difference between ΔS_{high} and ΔS_{low} was found to be the lowest for the ONIOM2-(mPW1PW91/6-311G**:PM3) method with a value of −0.08 kcal/mol. Inclusion of diffuse function in the basis set, namely ONIOM2-(mPW1PW91/6-31+G**:PM3) yielded a higher value for ΔD = 0.35 kcal/mol. Interestingly, both of these values are well within the recommended error tolerance limit of 2 kcal/mol.[25] The energies were further refined through single-point energy calculations at the DFT//ONIOM level.[27] The lowest energy conformer, obtained through a detailed conformational analysis,[28] was subjected to geometry optimization using full DFT at the mPW1PW91/6-311G** level of theory without any partition scheme. The agreement between the DFT and ONIOM2 geometries was found to be impressively good, suggesting that ONIOM2 geometries are reliable for the present system.[29]

dx.doi.org/10.1021/jo301483p | J. Org. Chem. 2012, 77, 10525−10536

RESULTS AND DISCUSSION

The results and discussions are broadly grouped into (a) conformational analysis of the thiourea−cinchona unit and (b) mechanistic and stereoselectivity aspects of asymmetric decarboxylative protonation. While the conformational mapping of other thiourea derivatives has been reported previously, such studies on epicinchonidine thiourea systems are not widely known. Hence, we decided to disclose the key conformational features of the catalyst template first before describing the mechanism of asymmetric protonation.

1. Conformational Analysis. The initial recognition of the substrate by the hybrid thiourea cinchona framework is vital to the success of the subsequent reaction. When the catalyst itself can exist in a multitude of conformers, a detailed conformational analysis is desirable to be able to identify meaningful geometries of such inclusion complexes. The conformers of the cinchona family of alkaloids are generally classified into *Closed* and *Open* forms. In *Closed* conformers, the lone pair of quinuclidine nitrogen is oriented toward the quinoline ring, whereas in *Open* conformers, the lone pair points away from the quinoline moiety. A combination of computational and NMR experiments on cinchonidine identified as many as 11 unique conformers that differ in dihedral angles τ_1 and τ_2, termed as characteristic dihedral angles, as shown in Figure 2.[30] Besides such conformational features of cinchonidines previously known, the present system offers additional possibilities as the hydroxyl group of epicinchonidine is replaced by a thiourea moiety. The presence of an additional aryl group on the farther nitrogen of thiourea gives rise to even larger conformational landscape.

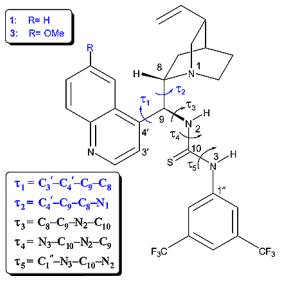

Figure 2. Key dihedral angles that are considered for the conformational analysis of epicinchonidine−thiourea derivative **1**.

Extensive conformational analysis of the epicinchonidine−thiourea catalyst is carried out at the ONIOM2(mPW1PW91/6-311G**:PM3) level of theory by varying the dihedral angles τ_1−τ_5, as shown in Figure 2.[31] As many as 44 different conformers are identified, and the energy distribution as a function of key dihedral angles is summarized in the form of a conformational map in Figure 3(ii). Each of these conformers is found to be a true minimum on the potential energy surface.[32] These conformer families include both *syn* and *anti* relative orientations of the N−H groups in thiourea. It is important to note that the catalytically active conformer is expected to remain in a *syn* arrangement for improved hydrogen bonding with the substrates.

The optimized geometries of a representative conformer from each major conformer families along with their characteristic dihedral angles (τ_1 and τ_2) are shown in Figure 3(i). The rotations about quinoline (τ_1) and quinuclidine (τ_2) moieties for fixed thiourea conformers (τ_3, τ_4, and τ_5) provided six different conformers with characteristic optimized τ_1 and τ_2 values. Successive rotations about τ_3, τ_4, and τ_5 with constant τ_1 and τ_2 values (more detailed illustration is provided in Scheme S1 in the Supporting Information) led to additional conformers within each such conformer family. The lower energy conformers indicate the presence of a relatively stronger intramolecular hydrogen bonding in *Open*(4) and partly in *Open*(3) families resulting in deeper wells on the potential energy surface. The dihedral angle τ_2 captures the effectiveness of intramolecular hydrogen bonding contact between the thiourea hydrogen and the quinuclidine nitrogen and hence exerts a pivotal effect on the relative energies of these conformers. The key dihedral angle τ_2 spanning 160−200° provides the two most stable conformer families *Open*(3) and *Open*(4). For relatively less stable conformer families such as *Open*(5) and *Open*(6), τ_2 is found to be in the range of −60° to −90°. Interestingly, conformers of similar energies could exhibit larger differences in τ_1 values.[33] The families *Open*(5), *Open*(6), *Closed*(1), and *Closed*(2) wherein the thiourea moiety is away from the quinuclidine nitrogen are found to remain on the higher energy terrain of the conformational landscape. The conformer families in the increasing order of energy is found to be *Open*(4) < *Open*(3) < *Closed*(1) < *Open*(6) < *Open*(5) < *Closed*(2). It is observed that the maximum number of conformers falling in the minimum energy range belong to *Open*(4). The conformer distribution of epicinchonidine-thiourea hybrid catalyst is identified to exhibit a general similarity with that of epiquinine, wherein *Open*(4) conformer was identified as the most preferred one.[34] Hence, the conformational space sampled could be similar to the related systems such as epicinchonidine and epiquinine thiourea derivatives as well. While this paper was under review, a related work partly mirroring the dual activation mechanism involving bifunctional cinchona−thiourea catalyst appeared in literature from Zhu et al.[35] Similar conformational features have been obtained by relaxed potential energy scan as well as variations in key dihedral τ_1 and τ_3.

Thiourea derivatives of epicinchonidine examined in this study offered interesting additional conformational features. The intramolecular hydrogen bonding between (i) the thiourea hydrogen and the quinuclidine nitrogen (d1), (ii) thiourea sulfur, and one of the *o*-aryl C−H groups (d2) are identified in different conformers (Figure 4). The latter interactions could offer a moderate increase in catalyst rigidity as compared to the parent epicinchonidine.[9b] Conformers possessing both these types of hydrogen bonds are found to be relatively more stabilized. A pictorial representation of the relationship between the computed energies and the hydrogen bonding distances (d1 and d2) that captures the change in weighted mean relative Gibbs free energy with respect to the variations in the key hydrogen bonding contacts is provided in Figure 4.[36] The various conformers with *syn* and *anti* relative orientations of the N−H groups of thiourea in all six different conformer families are studied. It is found that the most stable conformer is *open*4_7 with an *anti* relative orientation (Figure 3(i)). The intramolecular hydrogen bonding, as discussed above, renders improved stabilization for conformers with similar orientation in other conformer families as well.

Although *open*4_7 is the most stable conformer and would remain the most populated, another conformer *open*4_3, as shown in Figure 3(iii), with a *syn* relative orientation of the N−H groups is considered as the catalytically active conformer. The later conformer is the most preferred geometry with a *syn* disposition of the N−H groups. Mechanistic studies are therefore performed using this conformer owing to the availability of two

dx.doi.org/10.1021/jo301483p | J. Org. Chem. 2012, 77, 10525−10536

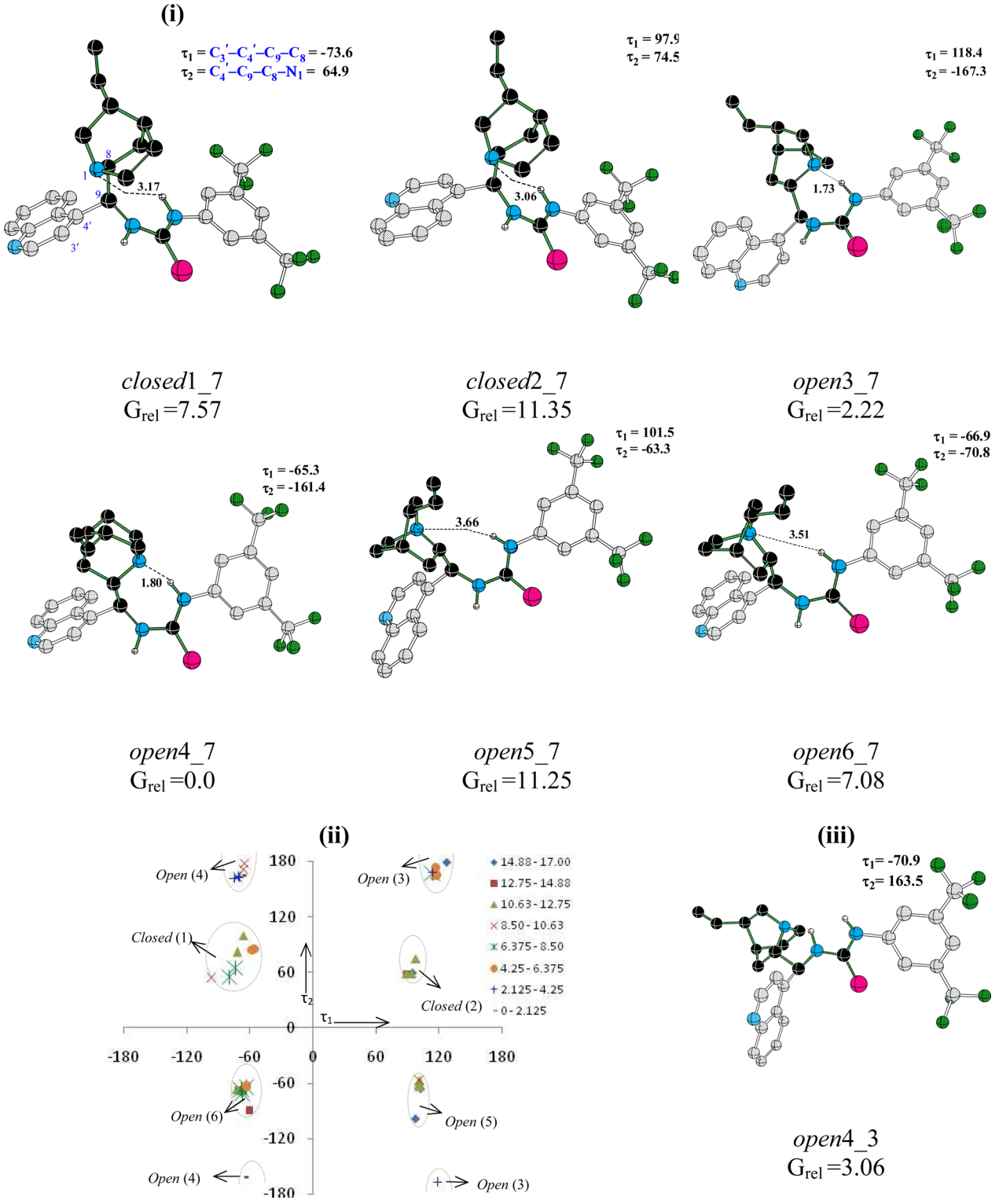

Figure 3. Conformers of epicinchonidine derivative **1** optimized at the ONIOM2(mPW1PW91/6-311G**: PM3) level each from six different conformer families (**i**). Characteristic dihedral angle ranges spanned by different conformers (**ii**). Lowest energy conformer *open*4_3 with a *syn* relative orientation of the N–H, which is the preferred catalytically active conformer (**iii**). (See Scheme S1, Supporting Information, for additional details on the nomenclature employed.)

hydrogen bond donor N–H groups that can bind the substrate well. A number of recent experimental and computational studies on different thiourea derivatives have employed conformers with a *syn* relative orientation of the N–H groups as the active conformer of the catalyst.[37]

2. Mechanistic Studies. It is important to recognize the preferred geometry of the catalyst–substrate binary complexes wherein further reaction takes place. In other words, there could be thermodynamic advantages prior to the kinetically significant step that controls stereoselectivity of the reaction. In the present

dx.doi.org/10.1021/jo301483p | J. Org. Chem. 2012, 77, 10525–10536

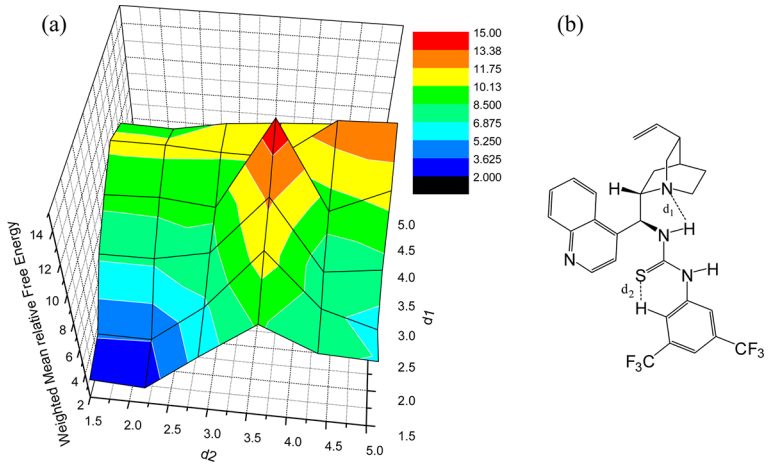

Figure 4. (a) Dependence of weighted mean relative Gibbs free energy (in kcal/mol) on the intramolecular hydrogen bonding (in 44 lower energy conformers of epicinchonidine-thiourea derivative). (b) Key hydrogen bonding contacts (d_1 and d_2).

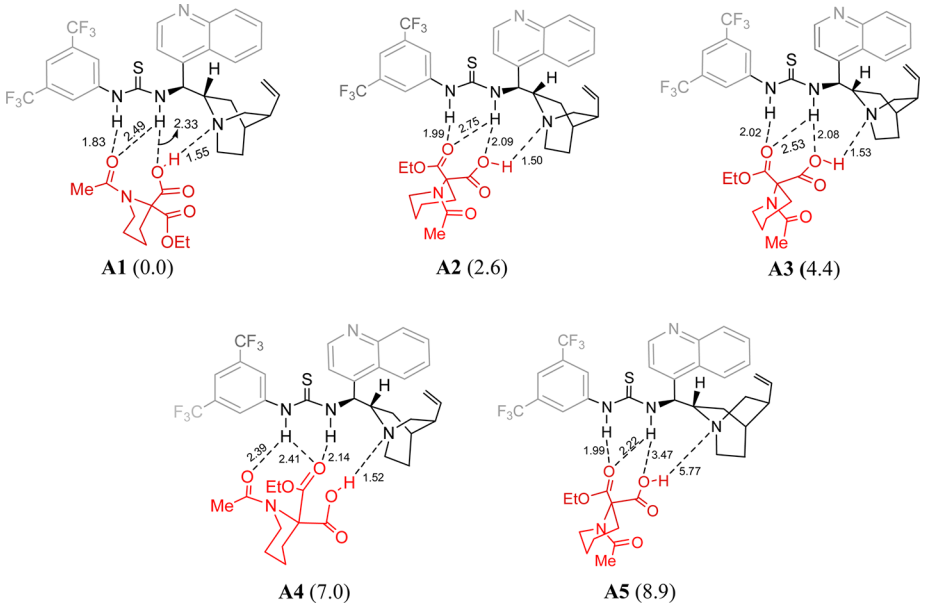

Figure 5. Various binary complexes of α-amino malonate hemiester (in red color) with the alkaloid derivative **1**. The relative energies (in kcal/mol) obtained at the ONIOM2(mPW1PW91/6-31+G**:PM3) level of theory are provided in parentheses. Distances are in Å.

context, a racemic mixture of α-amino malonate hemiester is the substrate that undergoes enantioselective decarboxylative protonation. A number of binary complexes of the *S* enantiomer and the thiourea−cinchona template are examined first. These binary adducts exhibit multiple hydrogen-bonding interactions, as readily evident from the optimized geometric parameters provided in Figure 5. Various likely binary adducts between *open*4_3 conformer and the substrate α-amino malonate hemiester, as depicted in Figure 5, are then examined. In a very recent study, Zhu et al. examined the mechanism of bifunctional cinchona−thiourea-catalyzed direct vinylogous Michael reaction of α,β-unsaturated γ-butyrolactam and chalcone. The preferred structure of the catalyst employed is of *Open*(4) type, similar to that noticed in this work.[35] Different kinds of hydrogen-bonding contacts between the thiourea donor N−H groups and various acceptor sites on the substrate are obtained by rotating the substrate followed by independent geometry optimization of such inclusion complexes (and characterization of such stationary points as true minima). This analysis led to binary complexes wherein the thiourea N−H group interacts with (a) ester carbonyl and the hydroxyl group in **A2** and **A3**, (b) amide carbonyl and the hydroxyl group in **A1**, (c) both the ester and the amide carbonyls in **A4**, and (d) only the ester carbonyl in **A5**. Except in **A5**, all other complexes exhibit hydrogen bonding interaction between the quinuclidine nitrogen and the carboxylic acid group on the substrate. The inclusion complex **A1** is found to be energetically the most preferred adduct. A number of such binary adducts have been identified within an energy range of 8.9 kcal/mol with respect to the lowest energy adduct.

It is important to note at this juncture that the best enantioselectivity was reported when epiquinine thiourea derivative **3** is employed as the catalyst.[15a] The only structural difference with epicinchonidine derivative (**1**) is in terms of the C_6' substituent in the quinoline ring. In epiquinine, the C_6' substituent is an $-OCH_3$ group, while it is unsubstituted in the parent epicinchonidine.[38] We have considered epiquinine thiourea hybrid catalyst **3** for the mechanistic investigation. The reaction can be envisaged to begin from the inclusion

dx.doi.org/10.1021/jo301483p | J. Org. Chem. 2012, 77, 10525−10536

Scheme 2. Three Different Mechanistic Pathways A–C for Asymmetric Decarboxylative Protonation of α-Amino Malonate Hemiester

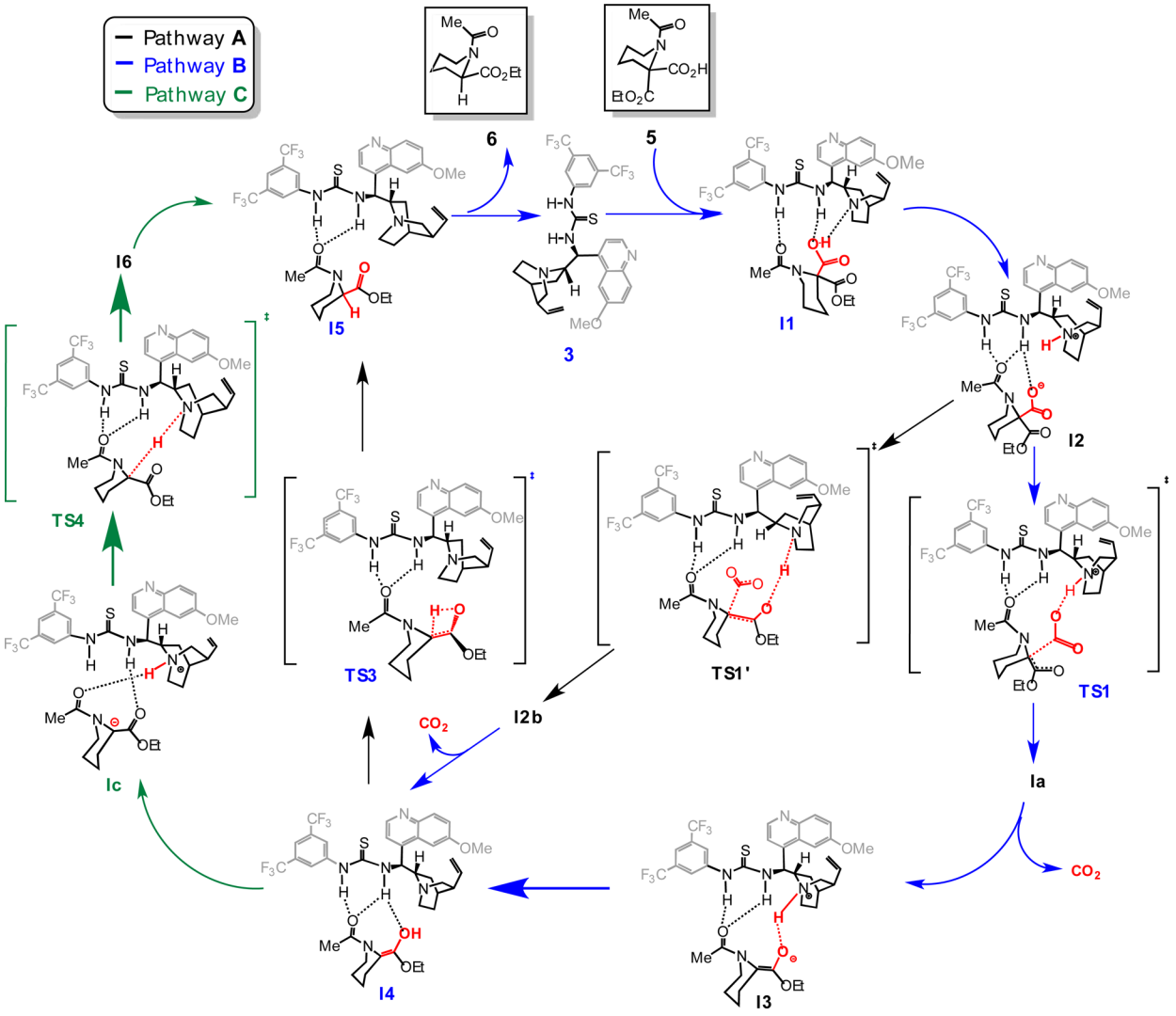

complex **I1** as shown in Scheme 2. The initial step involves an acid–base reaction wherein quinuclidine deprotonates the carboxylic acid of the substrate through a barrierless process to form intermediate **I2**. All of the discussions in the text use Gibbs free energies in the solvent phase (acetone) calculated by including the thermal and entropic terms obtained using the ONIOM2 method to the single-point energies at the M06-2X/6-311+G(d,p) level of theory.[39]

Akin to the catalyst–substrate inclusion complexes described earlier, a network of hydrogen-bonding interactions between the carbonyl oxygen of the amide as well as the carboxylate groups with the thiourea hydrogens is noticed in **I2**. In addition, the quinuclidinium proton interacts with the carboxylate group of the substrate. A similar binding mode in the thiourea–cinchona catalyst was recently reported in a Michael addition reaction as well.[35] Interesting and subtle mechanistic divergence emanates from **I2**. A concerted decarboxylation and protonation of the ensuing enolate via **TS1′** gives rise to pathway **A**, whereas a two-step decarboxylation to **I3** via **TS1** followed by a protonation of the ester enolate forms the premise for pathway **B**, shown in Scheme 2. It is evident from the optimized geometry of **TS1′** in pathway **A** that the expulsion of carbon dioxide is accompanied by the transfer of quinuclidinium proton to the oxygen of the ester enolate (Figure 6).[40] The conformational flexibility allows a large change in τ_2 value from 148° in the starting binary complex **I2** to −157.6° in **TS1′** such that the quinuclidinium proton can be transferred to the ester carbonyl. Complete removal of CO_2 then yields intermediate **I4** which is an enol form of the decarboxylated substrate. The major issue with pathway **A** herein presented relates to the higher energy of the decarboxylation transition state **TS1′**. The Gibbs free energy of **TS1′** is as high as 50 kcal/mol with respect to the separated reactants, implying that the removal of CO_2 is unlikely to proceed through this route. This situation prompted us to examine an alternative possibility denoted as pathway **B**, which is presented in the following section.

The major difference between pathways **A** and **B** pertains to the timing of protonation of the developing enolate formed as a result of the removal of carboxylate in the form of CO_2. In **TS1**, the critical C–C bond distance between the departing CO_2 and the substrate is 2.38 Å. The decarboxylation is found to be ahead of protonation in the case of pathway **B**. The Gibbs free energy of the transition state for decarboxylation in pathway **B** (**TS1**) is 16.5 kcal/mol lower than the corresponding transition state in pathway **A** (**TS1′**). The quinuclidinium proton offers additional stabilization to **TS1** through an effective short distance hydrogen

dx.doi.org/10.1021/jo301483p | J. Org. Chem. 2012, 77, 10525–10536

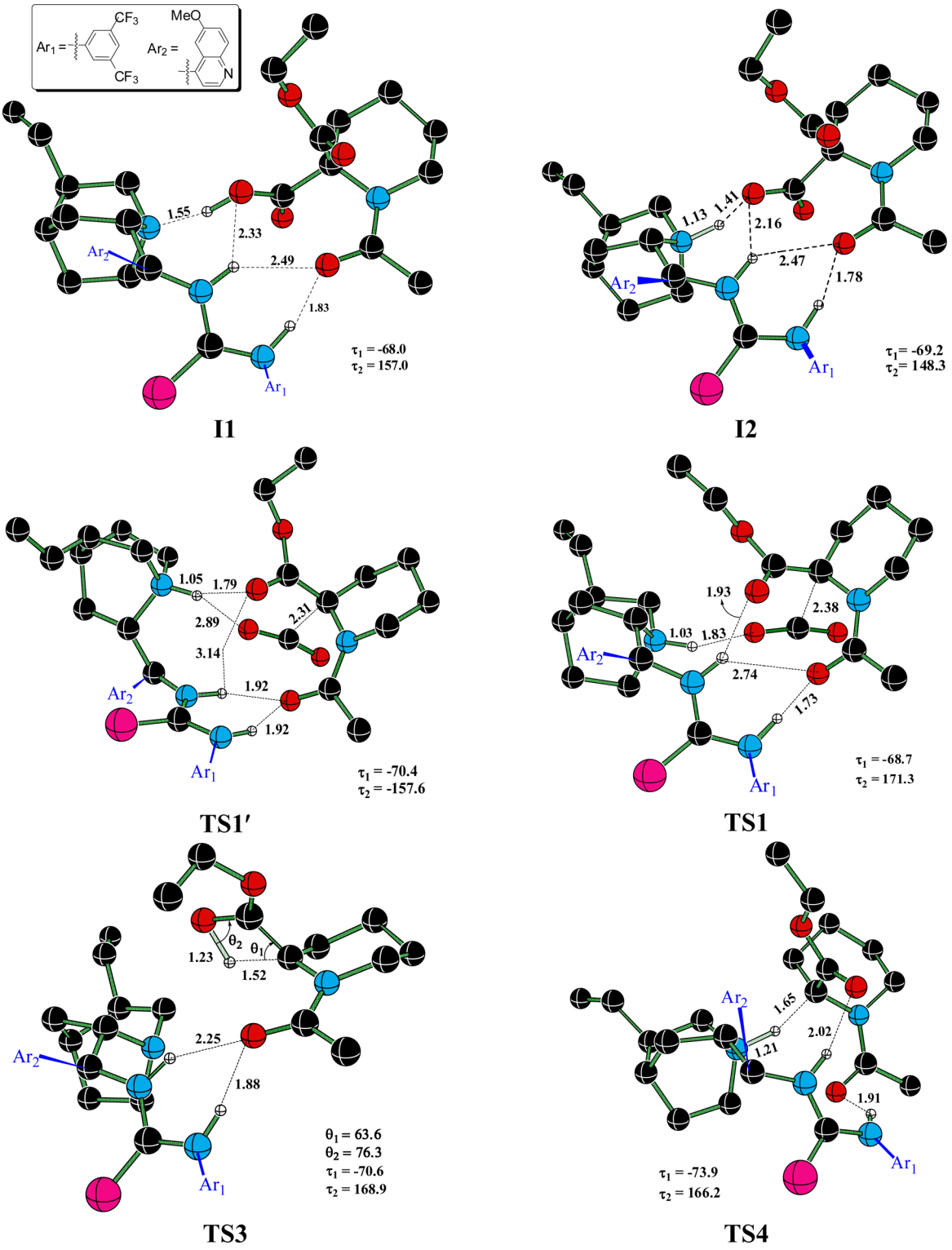

Figure 6. Optimized geometries of important binary complexes and the transition states involved in various mechanistic pathways. Distances are in angstroms and angles in degrees. Only select hydrogens are shown.

bonding with the departing CO_2. Furthermore, the resulting enolate is also stabilized through hydrogen bonding by the thiourea framework. The substrate orientation is different in these transition states, as evident from the τ_2 values in **TS1** and **TS1′** (Figure 6). A larger conformational change is desirable from preceding intermediate **I2** to **TS1′** to enable simultaneous protonation of the resulting enolate as the decarboxylation progresses. The enolate **I3** thus generated in pathway **B** would abstract the quinuclidinium proton to furnish enol intermediate **I4**.[41] The enol **I4** then undergoes keto−enol tautomerization through a relatively higher energy transition state **TS3** to give intermediate **I5**, which is a product complex between the chiral decarboxylated product bound to the catalyst template.

dx.doi.org/10.1021/jo301483p | J. Org. Chem. 2012, 77, 10525−10536

A closer perusal of the computed energetics indicates that the tautomerization transition state **TS3** is of fairly higher energy (69.0 kcal/mol). While the mechanism involving the protonation of the enolate oxygen by quinuclidinium proton (pathways **A** and **B**) at the first place appears reasonable, a high energy strained four-membered tautomerization transition state suggests that these two pathways are less likely to operate (Table 1).

Table 1. Relative Energies[a] of Key Stationary Points Involved in Pathways A–C in the Condensed Phase (Acetone) Obtained Using the Geometries at the ONIOM2(mPW1PW91/6-31+G: PM3) Level of Theory**

	ΔG_{sol}		
stationary points	$SMD_{(acetone)}$/mPW1PW91/6-31+G**	$SMD_{(acetone)}$/M06-2X/6-31+G**	$SMD_{(acetone)}$/M06-2X/6-311+G**
I1	11.1	3.5	3.8
I2	10.0	2.7	2.8
TS1′	59.9	52.1	50.4
I2b	47.3	39.1	36.8
TS1	45.2	36.2	33.9
I3	27.8	20.5	17.5
TS2	–[b]–	–[b]–	–[b]–
I4	39.2	34.7	32.4
TS3	69.1	71.4	69.0
I5	−6.5	−3.8	−6.9
Ia	35.4	25.8	22.9
Ic	14.9	10.2	7.3
TS4	29.4	22.2	19.5
I6	12.8	5.3	2.2

[a]All energies (kcal/mol) are relative to infinitely separated reactants. [b]The TS could not be located even after repeated attempts.

Tautomerization transition states are known to enjoy additional stabilization in polar protic solvents[42] due to the potential involvement of a solvent-assisted proton shuttle. However, it is less likely under the reaction conditions employed in this reaction, which involves aprotic solvents like acetonitrile, acetone, or THF. However, a finite possibility of moisture in reagents cannot be fully ruled out. We have therefore carried out additional computations with an explicitly included water molecule, both in a passive- and active-assisted mode. It is observed that the transition states for the passive-assisted mode wherein water is bound to oxygen in a keto–enol tautomerization are found to be about 3.5 kcal/mol higher energy than in the absence of water. An active-assisted pathway involving a relay proton transfer could not be identified even after repeated attempts. The water molecule tends to depart away from the site of reaction during the course of geometry optimization. The available space for the inclusion of water appeared unfavorable, implying that such pathways are unlikely to remain significant.

The above-mentioned situation led us to consider an alternative pathway wherein the protonation of the enolate carbon, instead of oxygen, is considered. Most of the elementary steps in this route, depicted as pathway **C** in Scheme 2, are similar to the earlier possibilities. The major difference here relates to the mode of proton transfer from the quinuclidinium nitrogen. Instead of a two-step proton transfer via an enol intermediate (**I3** and **I4** in the earlier pathways), a direct protonation of the carbon atom bearing the ester group holds the key to pathway **C**.

The major advantage of pathway **C** is that it circumvents the involvement of a higher energy keto–enol tautomerization transition state **TS3**. Here, the decarboxylation occurs through **TS1** resulting in **I3**, which is then protonated by the quinuclidinium ion to **I4**. Although the ester enolate of the substrate bound to the protonated amine, in both **I3** and **Ic** are structurally similar, the latter is found to be of lower energy due to the differences in the alkaloid conformation as well as in the interactions between the enolate and the thiourea hydrogens.[43] Besides a facile and unhindered proton transfer, the transition state **TS4** for protonation of the enolate carbon exhibits multiple stabilizing interactions such as $H_{thiourea}\cdots O_{carbonyl}$ that results in lowering of energy to 19.5 kcal/mol (Figure 7). In the resulting intermediate **I6** the ester and amido carbonyl groups interact with the thiourea moiety. **I6** then undergoes a minor change in its orientation and the hydrogen bonding so as to proceed to a relatively more stable complex **I5**, which upon removal from the thiourea furnishes the final product.

A more direct comparison between all three pathways for asymmetric decarboxylative protonation of α-amino malonate hemiester can be drawn from the energy profile diagram generated at the $SMD_{(acetone)}$/M06-2X/6-311+G**//ONIOM2 level of theory (Figure 7). It can be noticed that pathway **A** suffers from a higher energy decarboxylation step while pathway **B** encounters a higher energy tautomerization. Interestingly, the Gibbs free energy for the direct proton transfer transition state is much lower than that in other pathways,

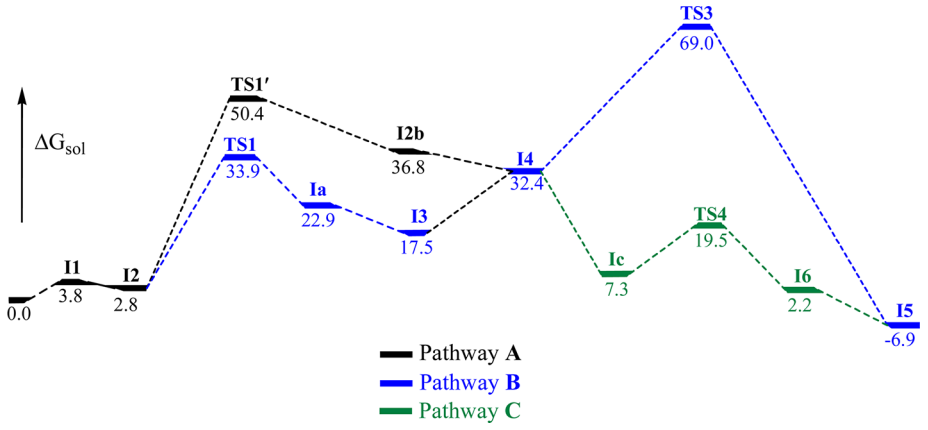

Figure 7. Gibbs free energy profile (in kcal/mol) generated at the M06-2X/6-311+G**//ONIOM2(mPW1PW91/6-31+G**:PM3) level of theory including solvent effect (acetone) for the pathways **A**–**C** via inclusion complex **I1**.

dx.doi.org/10.1021/jo301483p | J. Org. Chem. 2012, 77, 10525–10536

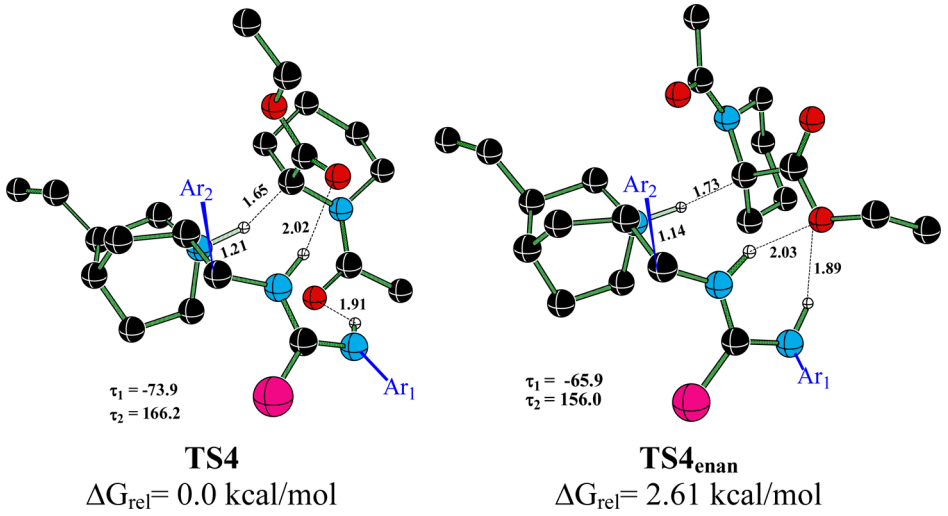

Figure 8. Diastereomeric transition states for the direct protonation of the enolate carbon in pathway **C**.

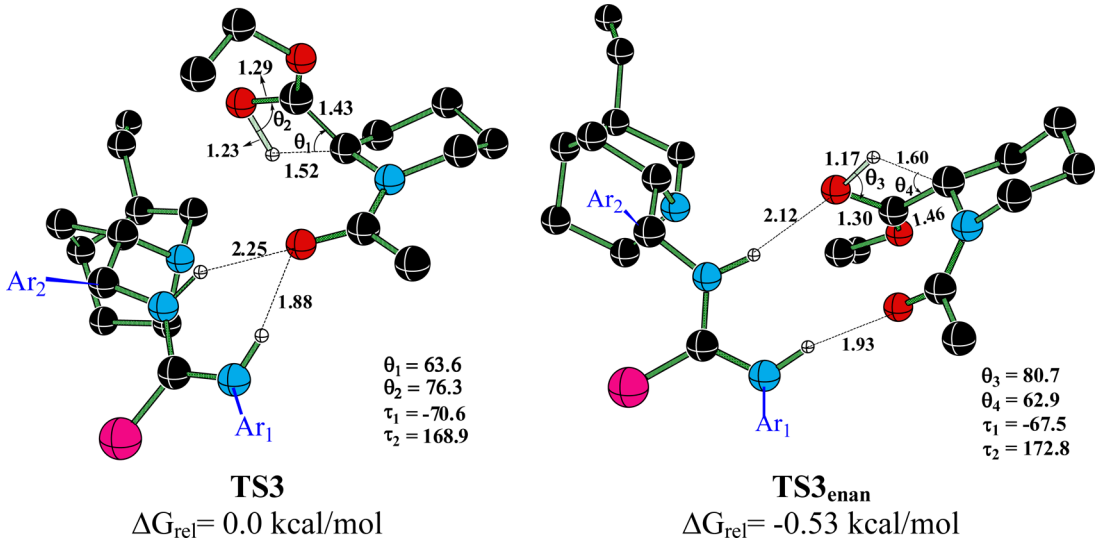

Figure 9. Diastereoselective transition states involved in pathways **A** and **B**.

suggesting that the reaction is most likely to proceed through pathway **C**.

Thus far, the reaction is considered to emanate from the energetically most favored binary complex **I1**, which is the epiquinine analogue of **A1**. To examine how the computed energetics in pathway **C** would be, with a higher energy inclusion complex such as **I1′** (**A2** analogue as shown in Figure 5), we have investigated the key steps of the reaction by choosing **I1′** as the starting point. It is identified that the decarboxylation barrier is higher in the case of inclusion complex **I1′** as compared to that from **I1**. Thus, the asumption that the reaction is most likely to proceed from the energetically more favored inclusion complex is valid in the present example.[44]

After having identified the energetically preferred pathway, we turned our attention to the critical step responsible for stereoselectivity in this reaction. Since the computed energetics are very much in favor of pathway **C**, emphasis here is placed on the direct protonation of enolate carbon. As described in the previous section, a direct protonation of the enolate carbon through **TS4** holds the key to the stereochemical outcome. The quinuclidinium proton can be delivered to the enolate carbon through either of its the prochiral faces, each giving rise to distinct enantiomeric products. The critical question at this juncture is therefore to identify the facial preference for the asymmetric proton transfer. **TS4**$_{enan}$ is found to be higher by 2.6 kcal/mol than its diastereomeric pair **TS4** (Figure 8). This situation suggests that the most preferred stereoisomer would be formed via the direct protonation transition state **TS4** resulting in the *R* enantiomer as the final product. An energy difference of this order corresponds to an enantiomeric excess of 97.5%, which is in good agreement with the experimental observation of 89% ee in favor of the *R* enantiomer.[15a] It is therefore gratifying to note that the transition state model herein suggested as the key to asymmetric protonation is quite effective toward rationalizing the stereochemical outcome of this interesting reaction.

The optimized geometries of these stereocontrolling transition states are provided in Figure 8. The strength and pattern of hydrogen bonding is found to be different in these two transition states. In the case of the lower energy transition state **TS4**, both amido and ester carbonyl groups of the substrate maintain hydrogen bonding contacts with the N−H groups of the thiourea moiety. However, only the ethoxy oxygen of the ester group is hydrogen bonded to thiourea in diastereomeric **TS4**$_{enan}$. A carbonyl oxygen is a better hydrogen bond acceptor than an ether

dx.doi.org/10.1021/jo301483p | *J. Org. Chem.* 2012, 77, 10525−10536

oxygen. The difference in strength of interactions contributes to the vital energy difference responsible for stereoselectivity. In the case of pathways **A** and **B**, the enolization transition state **TS3** is responsible for asymmetric protonation. The proton can be added either from above or below the average plane, resulting in the two enantiomeric forms (Figure 9). The energy difference between the diastereomeric transition states (**TS3** and $\mathbf{TS3}_{enan}$) is found to be as little as −0.53 kcal/mol, suggesting a very low enantioselectivity through this route (40% ee) with a sense of enantioselectivity opposite to what has been earlier noticed experimentally. Furthermore, the lower energy transition state corresponds to an incorrect enantiomer as compared to experimental observation. These predictions offer additional credence to the validity of pathway **C** as an operating mechanism and can be deemed responsible for enantioselective asymmetric decarboxylative protonation.

CONCLUSIONS

The relative energies of different conformer families of epicinchonidine thiourea hybrid organocatalyst (**1**) have been compared using different hybrid DFT:semiempirical two-layer ONIOM2 partition schemes. Among 12 such layering schemes, the ONIOM2(mPW1PW91/6-311G**:PM3) combination has been identified as exhibiting best geometric as well as energetic agreement with that of full DFT computations. A detailed conformational analysis of this hybrid catalyst yielded 44 different conformers spread across six different conformer families within an energy range of 16 kcal/mol. An active catalyst conformer with a *syn* relative disposition of the thiourea N−H groups is employed for mechanistic studies wherein the substrate fit well through hydrogen bonding interaction while the quinuclidine activates the pro-nucleophile. Mechanistic investigations on asymmetric protonation of α-amino malonate hemiester promoted by epiquinine−thiourea hybrid (**3**) has revealed interesting mechanistic pathways. The mechanism is identified to involve bifunctional action of the catalyst template on the substrate, first by the formation of an inclusion complex between the substrate and the thiourea backbone facilitated by the thiourea N−H groups acting as hydrogen bond donors. Next, deprotonation of the carboxylic acid group of the substrate by the quiniclidine nitrogen would provide a carboxylate intermediate. The decarboxylation of the β-keto carboxylate intermediate is identified as the likely rate-limiting step of the reaction. In the energetically most preferred pathway, the vital asymmetric protonation occurs through the transfer of proton from the chiral quinuclidinium directly to the enolate carbon (pathway **C**), while the substrate is held by the thiourea moiety. Alternative pathways, wherein the transfer of quinuclidinium proton to the enolate oxygen followed by keto−enol tautomerization (pathways **A** and **B**) have been found to encounter higher barriers. The differential hydrogen bonding between the chiral epicinchona-thiourea moiety and the prochiral enolate in the diastereomeric transition states has been recognized as responsible for high enantioselectivity in the reaction. The predicted sense and extent of enantioselectivity has been found to be in very good agreement with the experimental results.

ASSOCIATED CONTENT

Supporting Information

Additional details of computational methods, complete citation of ref 21, optimized Cartesian coordinates of various intermediates, transition states along with their energies, and other pertinent details. This material is available free of charge via the Internet at http://pubs.acs.org.

AUTHOR INFORMATION

Corresponding Author

*Fax: +91 22 2576 7152. E-mail: sunoj@chem.iitb.ac.in.

Notes

The authors declare no competing financial interest.

ACKNOWLEDGMENTS

Generous computing time from the IIT Bombay computer center is gratefully acknowledged. A.S. acknowledges UGC (New Delhi) for a Junior Research Fellowship; and Garima Jindal and Yernaidu Reddi (IIT Bombay) for their help during the revision of this manuscript.

REFERENCES

(1) (a) Marcelli, T.; Hiemstra, H. *Synthesis* **2010**, *8*, 1229. (b) Marcelli, T. *WIREs Comp. Mol. Sci.* **2011**, *1*, 142.
(2) (a) Dijkstra, G. D. H.; Kellogg, R. M.; Wynberg, H. *J. Org. Chem.* **1990**, *55*, 6121. (b) Schurch, M.; Schwalm, O.; Mallat, T.; Weber, J.; Baiker, A. *J. Catal.* **1997**, *169*, 275. (c) Burgi, T.; Vargas, A.; Baiker, A. *J. Chem. Soc., Perkin Trans. 2* **2002**, 1596.
(3) Denmark, S. E.; Beutner, G. L. *Angew. Chem., Int. Ed.* **2008**, *47*, 1560.
(4) (a) Hiemstra, H.; Wynberg, H. *J. Am. Chem. Soc.* **1981**, *103*, 417. (b) Cucinotta, C. S.; Kosa, M.; Melchiorre, P.; Cavalli, A.; Gervasio, F. L. *Chem.—Eur. J.* **2009**, *15*, 7913.
(5) (a) Taylor, M. S.; Jacobsen, E. N. *Angew. Chem., Int. Ed.* **2006**, *45*, 1520. (b) Doyle, A. G.; Jacobsen, E. N. *Chem. Rev.* **2007**, *107*, 5713. (c) Knowles, R. R.; Jacobsen, E. N. *Proc. Natl. Acad. Sci. U.S.A.* **2010**, *107*, 20678.
(6) (a) Schreiner, P. R. *Chem. Soc. Rev.* **2003**, *32*, 289. (b) Pihko, P. M. *Angew. Chem., Int. Ed.* **2004**, *43*, 2062.
(7) Etter, M. C.; Urbáczyk-Lipkowska, Z.; Zia-Ebrahimi, M.; Panunto, T. W. *J. Am. Chem. Soc.* **1990**, *112*, 8415.
(8) Sigman, M. S.; Jacobsen, E. N. *J. Am. Chem. Soc.* **1998**, *120*, 4901.
(9) (a) Schreiner, P. R.; Wittkopp, A. *Org. Lett.* **2002**, *4*, 217. (b) Schreiner, P. R.; Wittkopp, A. *Chem.—Eur. J.* **2003**, *9*, 407.
(10) Okino, T.; Hoashi, Y.; Takemoto, Y. *J. Am. Chem. Soc.* **2003**, *125*, 12672.
(11) Li, B. J.; Jiang, L.; Liu, M.; Chen, Y. C.; Ding, L. S.; Wu, Y. *Synlett* **2005**, 603.
(12) Vakulya, B.; Varga, S.; Csámpai, A.; Soós, T. *Org. Lett.* **2005**, *7*, 1967.
(13) (a) Marcelli, T.; van Maarseveen, J. H.; Hiemstra, H. *Angew. Chem.* **2006**, *118*, 7658; *Angew. Chem., Int. Ed.* **2006**, *45*, 7496. (b) Connon, S. J. *Chem. Commun.* **2008**, 2499.
(14) (a) Zuend, S. J.; Jacobsen, E. N. *J. Am. Chem. Soc.* **2009**, *131*, 15358. (b) Zuend, S. J.; Jacobsen, E. N. *J. Am. Chem. Soc.* **2007**, *129*, 15872. (c) Hamza, A.; Schubert, G.; Soos, T.; Papai, I. *J. Am. Chem. Soc.* **2006**, *128*, 1315. (d) Hammar, P.; Marcelli, T.; Hiemstra, H.; Himo, F. *Adv. Synth. Catal.* **2007**, *349*, 2537.
(15) (a) Amere, M.; Lasne, M. C.; Rouden, J. *Org. Lett.* **2007**, *9*, 2621. (b) Blanchet, J.; Baudoux, J.; Amere, M.; Lasne, M. C.; Rouden, J. *Eur. J. Org. Chem.* **2008**, 5493.
(16) Mohr, J. T.; Hong, A. Y.; Stolt, B. M. *Nature Chem.* **2009**, *1*, 359.
(17) (a) Janardanan, D.; Sunoj, R. B. *J. Org. Chem.* **2007**, *72*, 331. (b) Shinisha, C. B.; Sunoj, R. B. *Org. Biomol. Chem.* **2008**, *6*, 3921. (c) Patil, M. P.; Sharma, A. K.; Sunoj, R. B. *J. Org. Chem.* **2010**, *75*, 731.
(18) (a) Warshel, A.; Levitt, M. *J. Mol. Biol.* **1976**, *103*, 227. (b) Singh, U.; Kollman, P. *J. Comput. Chem.* **1986**, *7*, 718. (c) Field, M. J.; Bash, P. A.; Karplus, M. *J. Comput. Chem.* **1990**, *11*, 700. (d) Aqvist, J.; Warshel, A. *Chem. Rev.* **1993**, *93*, 2523. (e) Billeter, S. R.; Webb, S. P.; Iordanov, T.; Agarwal, P. K.; Hammes-Schiffer, S. *J. Chem. Phys.* **2001**, *114*, 6925.

(19) (a) Cui, Q.; Guo, H.; Karplus, M. *J. Chem. Phys.* **2002**, *117*, 5617. (b) Gogonea, V.; Westerhoff, L. M.; Merz, K. M., Jr. *J. Chem. Phys.* **2000**, *113*, 5604.
(20) (a) Dapprich, S.; Komáromi, I.; Byun, K. S.; Morokuma, K.; Frisch, M. J. *THEOCHEM* **1999**, *1*, 461. (b) Vreven, T.; Morokuma, K. *J. Comput. Chem.* **2000**, *21*, 1419. (c) Morokuma, K. *Philos. Trans. R. Soc. London, Ser. A* **2002**, *360*, 1149. (d) Vreven, T.; Byun, K. S.; Komáromi, I.; Dapprich, S.; Montgomery, J. A., Jr.; Morokuma, K.; Frisch, M. J. *J. Chem. Theory Comput.* **2006**, *2*, 815.
(21) Frisch, M. J. et al. Gaussian 09, Revision A.02, Gaussian, Inc., Wallingford, CT, 2009 (see the Supporting Information for the full citation).
(22) A detailed computational method is given in the Supporting Information.
(23) (a) Dudding, T.; Houk, K. N. *Proc. Natl. Acad. Sci. U.S.A.* **2004**, *101*, 5770. (b) Shinisha, C. B.; Sunoj, R. B. *Org. Lett.* **2009**, *11*, 3242. (c) Brookes, N. J.; Ariafard, A.; Stranger, R.; Yates, B. F. *Chem.—Eur. J.* **2010**, *16*, 8117. (d) Su, Z.; Lee, H. W.; Kim, C. K. *Org. Biomol. Chem.* **2011**, *9*, 6402. (e) Anstaett, P.; Schoenebeck, F. *Chem.—Eur. J.* **2011**, *17*, 12340.
(24) (a) Morokuma, K. *Bull. Korean Chem. Soc.* **2003**, *24*, 797. (b) The S value is defined as $S_{(\text{level})} = E_{(\text{level, real})} - E_{(\text{level, model})}$ and the error associated with the ONIOM extrapolation; ΔD is therefore given by $(E_{(\text{high, real})} - E_{(\text{ONIOM})})$.
(25) See Table S1 in the Supporting Information for full details.
(26) Marenich, A. V.; Cramer, C. J.; Truhlar, D. G. *J. Phys. Chem. B* **2009**, *113*, 6378.
(27) See Tables S1 and S2 in the Supporting Information for additional details.
(28) The conformer *open*4_7 is found to be the most stable conformer of epicinchonidine derivative **1** at the ONIOM2(mPW1PW91/6-311G**:PM3) level of theory.
(29) See Figure S3 in the Supporting Information wherein the DFT and ONIOM2(mPW1PW91/6-311G**:PM3) are overlaid to bring out the mutual geometric agreement.
(30) Urakawa, A.; Meier, D. M.; Rüegger, H.; Baiker, A. *J. Phys. Chem. A* **2008**, *112*, 7250.
(31) A detailed description of conformational sampling methods employed in this study is provided in the Supporting Information.
(32) The energy values and the corresponding characterstic dihedral angles τ_1 and τ_2 are provided in Table S3 in the Supporting Information.
(33) Full details of energies of various conformer families and the characteristic dihedral angles are provided in Table S4 in the Supporting Information.
(34) Dijkstra, G. D. H.; Kellogg, R. M.; Wynberg, H.; Svendsen, J. S.; Marko, I.; Sharpless, K. B. *J. Am. Chem. Soc.* **1989**, *111*, 8069.
(35) Zhu, J.-L.; Zhang, Y.; Liu, C.; Zheng, A.-M.; Wang, W. *J. Org. Chem.* **2012**, *77*, 9813.
(36) See Table S4 in the Supporting Information for more details on the data employed in generating this map.
(37) (a) Hamza, A.; Schubert; Soós, G.; T.; Pápai, I. *J. Am. Chem. Soc.* **2006**, *128*, 13151. (b) Fu, A.; Thiel, W. *THEOCHEM* **2006**, *7*, 45. (c) Zuend, S. J.; Jacobsen, E. N. *J. Am. Chem. Soc.* **2007**, *129*, 15872. (d) Zuend, S. J.; Jacobsen, E. N. *J. Am. Chem. Soc.* **2009**, *131*, 15358. For the X-ray structures of thiourea derivatives employed as catalysts, see: (e) Li, B. L.; Wang, Y. F.; Luo, S. P.; Zhong, A. G.; Li, Z. B.; Du, X. H.; Xu, D. Q. *Eur. J. Org. Chem.* **2010**, 656. (f) Okino, T.; Hoashi, Y.; Furukawa, T.; Xu, X.; Takemoto, Y. *J. Am. Chem. Soc.* **2005**, *127*, 119.
(38) (a) The stability order for the binary complexes in the case of catalyst **3** is found to be of the same order as noticed for **1**. (b) Conformational features also remain the same between these two catalysts. See Table S5 in the Supporting Information.
(39) The thermal and entropic contributions were evaluated at the ONIOM2(mPW1PW91/6-31+G(d,p): PM3) level of theory using standard statistical mechanics approaches within the harmonic oscillator and rigid rotor approximations.
(40) Intrinsic reaction coordinate (IRC) calculations confirm that the proton transfer is concomitant with the removal of CO_2.
(41) (a) A 1.64 kcal/mol lower rotamer of **TS1**, **TS1rot** was also identified, where the −OEt group is toward the thiourea moiety while the carboxyl group is away from the quinuclidine (Figure S5, Supporting Information). However, the energies calculated at the ONIOM2(mPW1PW91/6-31+G(d,p): PM3) level of theory were favorable for **TS1** over the rotamer, and thus, we went on with the reaction pathway resulting from **I4** as the enol intermediate. (b) The transition state for proton abstraction could not be located even after multiple attempts with varying initial guess geometries. A subsequent scan of the potential energy surface in this region hints at the involvement of a barrierless protonation. See Figure S6 in the Supporting Information.
(42) Sunoj, R. B.; Anand, M. *Phys. Chem. Chem. Phys.* **2012**, *14*, 12715.
(43) Optimized geometries of intermediates **I3** and **Ic** are provided in Figure S7 in the Supporting Information.
(44) See Scheme S2, Figure S9, and Table S8 in the Supporting Information for additional details on this pathway.